

Short communication

Hetero-mixed TiO₂-SnO₂ interfaced nano-oxide catalyst with enhanced activity for selective oxidation of furfural to maleic acid

Petrus M. Malibo^{a,b}, Peter R. Makgwane^{a,b,*}, Priscilla G.L. Baker^b

^a Centre for Nanostructures and Advanced Materials (CeNAM), Council for Scientific and Industrial Research (CSIR), Pretoria 0001, South Africa

^b Department of Chemistry, University of the Western Cape, Robert Sobukwe Drive, Private Bag X17, Bellville 7535, South Africa



ARTICLE INFO

Keywords:

Heterostructure oxide
Tin dioxide
Titanium dioxide
Oxidation
Furfural

ABSTRACT

Herein we report on the catalytic activity of hetero-mixed TiO₂-SnO₂ nano-oxide catalyst for the selective liquid-phase oxidation of furfural to maleic acid using H₂O₂ oxidant. The high surface area and strong interaction of the two oxides with modified electronic structure manifested enhanced effective oxygen vacancies, and redox activity performance of the TiO₂-SnO₂ catalyst for furfural oxidation reaction. The structure of the catalyst was investigated by the powder X-ray diffraction (XRD), X-ray photoelectron spectroscopy (XPS), high-resolution transition electron microscopy (HRTEM), electron paramagnetic resonance (EPR) and Brunauer-Emmett-Teller (BET) surface area analyser techniques. The interfaced TiO₂-SnO₂ oxide catalyst was more catalytically active than its single counterpart SnO₂ and TiO₂ oxides to give a furfural conversion of 96.2% at up to 63.8% yield of maleic acid. The catalytic performance shown by TiO₂-SnO₂ present encouraging prospects for an economical solid metal oxide catalyst to access biobased maleic acid from renewable biomass-derived furfural.

1. Introduction

Selective oxidation of furfural to maleic acid and maleic anhydride is one of the important biomass conversion chemical processes in the production of renewable biobased chemicals [1]. Both maleic acid and maleic anhydride can be converted to bio-succinic acid, a precursor to 1,4-butanediol intermediate, which are both used in the synthesis of numerous biodegradable bioplastic polymers [2,3]. Industrially, the production of maleic acid is based on the maleic anhydride dehydration reaction process, which is accessed from the gas-phase oxidation of butane or benzene substrates over preferred V₂O₅ oxide based catalysts [4,5]. The process is fossil-based consisting of several energy intensive steps masked by co-production of green house gases such as CO₂ and CO, thus rendering the process economically costly and environmentally unfriendly [5].

Recently, there has been a growing interest in developing both liquid and gas-phase oxidation conversion of furfural to biobased maleic acid and maleic anhydride, respectively using H₂O₂ and molecular O₂ [6–9] (See Scheme 1). A bifunctional redox-acidic sites waste-derived poly(styrene sulphonic acid) catalyst has been designed and evaluated in the furfural oxidation to maleic acid using H₂O₂ oxidant to achieve a maleic acid yield of 34% [10]. The well-known epoxidation active catalyst,

titanium-silicate (TS-1) was evaluated for the oxidation of furfural with H₂O₂ to achieve maleic acid yield of 78% but the catalyst showed leaching, which affected its recycling activity [11]. Other heterogeneous solid catalysts have been studied for furfural oxidation with H₂O₂ and O₂ to maleic acid but still show low yields of maleic acid and/or poor recyclability [9,12,13]. Based on the previous reported catalytic activities of TiO₂ and SnO₂ in oxidation reactions [11,14,15], the design of their interfaced oxides together with the use of H₂O₂ could provide an access to economical synthesis route to biobased maleic acid from furfural oxidation. The activity enhancement effect of TiO₂-SnO₂ could result from Lewis acidic sites associated with both TiO₂ and SnO₂, including the Ti⁴⁺/Ti³⁺ redox reactivity and oxygen vacancies [16–20]. In this work, we demonstrate the enhanced catalytic activity of hetero-structure TiO₂-SnO₂ interfaced catalyst in the oxidation of furfural to maleic acid using H₂O₂. To understand the basis of the catalytic effect, the structure characteristics of the catalysts was studied by X-ray diffraction (XRD), X-ray photoelectron spectroscopy (XPS), electron paramagnetic resonance (EPR), high-resolution transition electron microscopy (HRTEM), and Brunner-Emmett-Teller (BET) nitrogen sorption techniques.

* Corresponding authors.

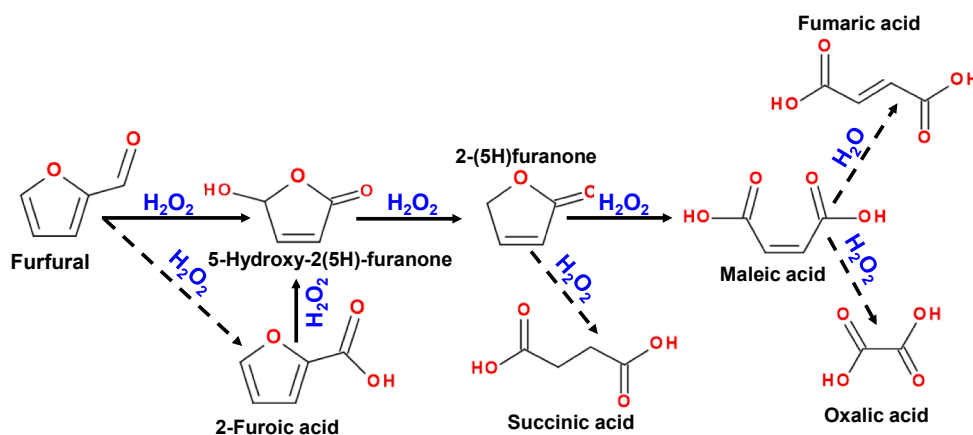
E-mail addresses: pmakgwane@csir.co.za, makgwane.peter@gmail.com (P.R. Makgwane).

<https://doi.org/10.1016/j.inoche.2021.108637>

Received 12 February 2021; Received in revised form 20 April 2021; Accepted 25 April 2021

Available online 29 April 2021

1387-7003/© 2021 Elsevier B.V. All rights reserved.



Scheme 1. Plausible reaction pathways for oxidation of furfural to intermediates, maleic acid and other products.

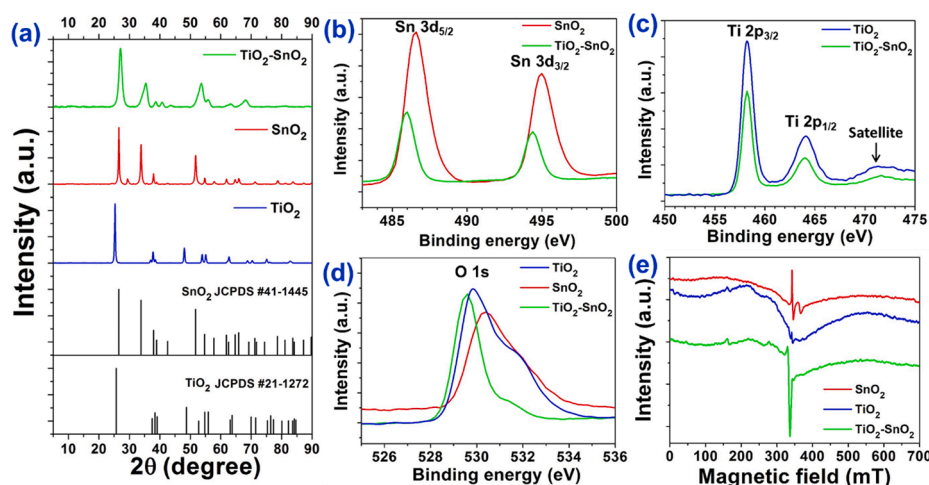


Fig. 1. Characterisation of $\text{TiO}_2\text{-SnO}_2$ catalyst. (a) XRD patterns; XPS spectra of (b) Sn 3d peaks, (c) Ti 2p peaks, (d) O 1s peaks; and (e) EPR profiles.

2. Experimental methods

The synthesis of the heterostructured $\text{TiO}_2\text{-SnO}_2$ and single SnO_2 and TiO_2 nano-oxide catalysts was carried by a solvothermal microwave-assisted heating method using solvent mixture of ethanol and ethylene glycol. The obtained and dried solids were calcined in a muffle furnace under air condition at a heating rate of $3\text{ }^\circ\text{C}/\text{min}$ from 30 to $500\text{ }^\circ\text{C}$ and held at $500\text{ }^\circ\text{C}$ for 4 h . The oxidation of furfural was carried out in a 25 ml flask fitted with a magnetic stirrer bar and a reflux condenser. Furfural (5 mmol), catalyst (100 mg) and co-solvent mixture (10 ml) of $5\text{ ml H}_2\text{O}$ and $5\text{ ml acetonitrile (CH}_3\text{CN)}$ were placed in the flask and H_2O_2 (25 mmol , 30% in H_2O) was added to the mixture. The flask was then quickly sealed with balloon and placed in a sand bath preheated to $60\text{ }^\circ\text{C}$ under reflux conditions. This mixture was then stirred continuously at 1000 rpm and kept at $60\text{ }^\circ\text{C}$ for 24 h . The separated liquid oxidation product from the solid catalysts was analysed by high performance liquid chromatography (HPLC). The elaborate catalysts synthesis and characterisation methods, including detailed oxidation products analysis are presented in the electronic supporting information (ESI).

3. Results and discussion

Fig. 1 summarizes the XRD, XPS and EPR characterisation results of the $\text{TiO}_2\text{-SnO}_2$ based catalysts. The XRD analysis confirmed the crystal structure and phase compositions of the $\text{TiO}_2\text{-SnO}_2$ interfaced catalyst

with respect to single TiO_2 and SnO_2 oxides as shown in **Fig. 1a**. SnO_2 is characterised by a tetragonal rutile structure with main peaks at 2θ of 26.9° , 34.2° and 51.8° together with additional peaks at 2θ of 29.3° and 36.3° , which are due to SnO [21]. The XRD of TiO_2 shows formation of the anatase phase. For $\text{TiO}_2\text{-SnO}_2$ catalyst, the TiO_2 peaks are not well resolved due to overlap with the SnO_2 peaks.

The XPS spectra of Sn 3d, Ti 2p and O 1s peaks of the heterostructure $\text{TiO}_2\text{-SnO}_2$ catalysts are illustrated in **Fig. 1b-d**. The Sn 3d spectrum of SnO_2 (**Fig. 1b**) shows the spin-orbit doublet corresponding respectively to $3d_{5/2}$ and $3d_{3/2}$ peaks of Sn^{4+} at 486.6 eV and 495.0 eV [22]. The Ti 2p of TiO_2 (**Fig. 1c**) display a spin-orbit doublet of peaks due to $2p_{3/2}$ and $2p_{1/2}$ at 458.6 eV and 464.2 eV and a satellite peak at 471.8 eV showing presence of Ti^{4+} [23]. The O 1s peak of SnO_2 at 530.4 eV indicate the existence of O^{2-} lattice oxygen atoms (**Fig. S2**) [24]. Both Sn 3d and O1s shows the peaks shifting respectively in $\text{TiO}_2\text{-SnO}_2$ to lower and higher BE regions (**Fig. 1a** and **d**). The peaks shifting is an indication of the strong interaction between TiO_2 and SnO_2 . The similar shifting of the XPS peaks observed in the heterostructure of $\text{TiO}_2\text{-SnO}_2$ catalyst has been reported to arise from the electrostatic and electronic effects [25–27]. In the case of $\text{TiO}_2\text{-SnO}_2$ hetero-interfaced catalyst, the higher electronegativity of Ti could results in electrons being pulled away from Sn toward Ti (i.e. strong Ti and Sn interaction referred to), and thus causing the peaks shifting which are accompanied by the modified electronic and chemical state.

Fig. 1e shows the EPR spectra of $\text{TiO}_2\text{-SnO}_2$ and its corresponding single oxides to investigate their interface effect on defects structure and

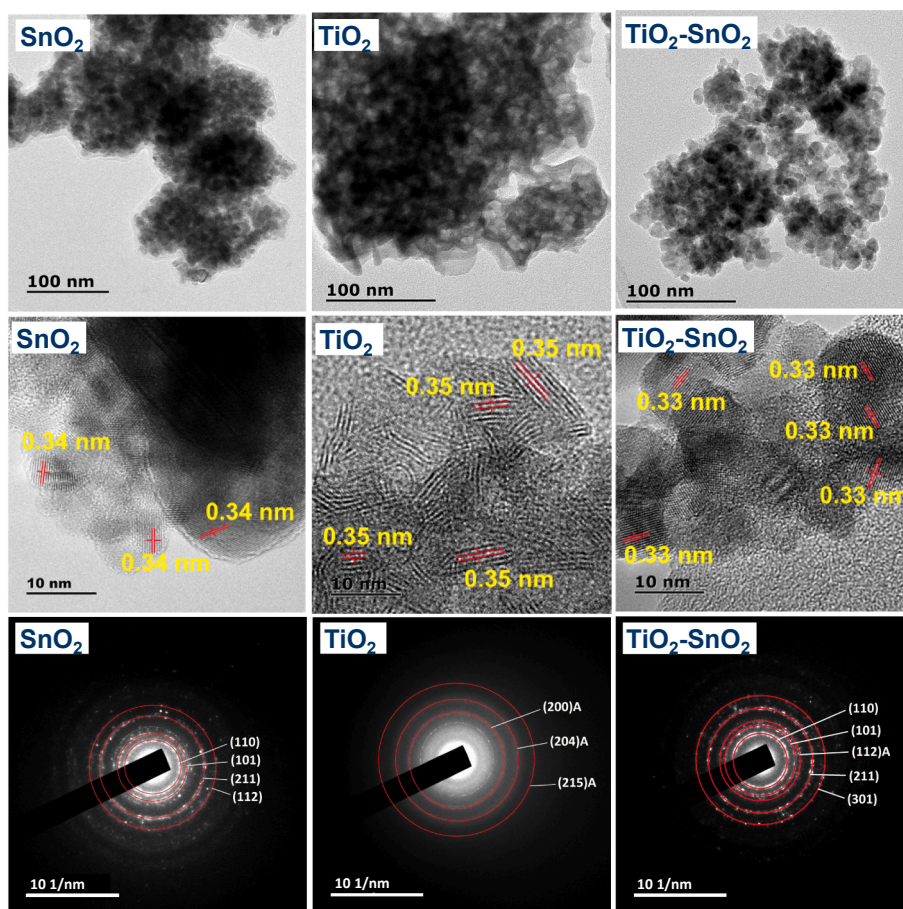


Fig. 2. TEM, SAED and HRTEM micrograph images of the $\text{TiO}_2\text{-SnO}_2$ catalysts.

Table 1

N_2 sorption and textural analysis of the $\text{TiO}_2\text{-SnO}_2$ catalysts.

| Catalysts | S_{BET} (m^2/g) | D_{pore} (nm) | V_{pore} (cm^3/g) | ^a Crystallite size (nm) |
|-----------------------------|--|------------------------|--|------------------------------------|
| SnO_2 | 13.2 | 9.5 | 0.031 | 6.1 |
| TiO_2 | 7.6 | 9.0 | 0.017 | 6.9 |
| $\text{TiO}_2\text{-SnO}_2$ | 72.6 | 11.0 | 0.20 | 5.9 |

^a determined by XRD using Scherrer equation. S_{BET} = surface area; D_{pore} = pore diameter; V_{pore} = pore volume.

oxygen vacancies properties. Both Sn^{4+} and Sn^{2+} cations are EPR silent thus, the observed signals for SnO_2 are due to the paramagnetic defect centres. These are confirmed by anisotropic resonance lines at $g = 1.971$, $g = 1.978$ and $g = 1.991$, which are attributed to the V_{O} paramagnetic centres created by the single-electron trapped inside the oxygen vacancies (V_{O}) [22]. The EPR signals for TiO_2 are due to the charge separation, which result from illumination at low temperature. These TiO_2 EPR photo-induced signals are at $g_1 = 1.951$, $g_2 = 1.993$ and $g_3 = 2.044$, respectively. The g_1 and g_2 are due to the electron trapping sites in the anatase/rutile phase of TiO_2 (lattice Ti^{3+}), while g_3 is assigned to the hole trapping sites (i.e. oxygen vacancies) [28,29]. The EPR of $\text{TiO}_2\text{-SnO}_2$ resembled that of TiO_2 , showing all the three g_1 , g_2 and g_3 resonance lines, thus indicating the high concentration amount of oxygen vacancies.

Fig. 2 show the TEM and HRTEM micrographs images of the heterostructure $\text{TiO}_2\text{-SnO}_2$ based catalysts. The SnO_2 showed to compose of agglomerated densely packed nanoparticles (NPs) with non-uniform shapes and sizes. For TiO_2 , the morphology shows the formation of densely packed agglomerates of short amorphous rod-like particles with a diameter range of about 4–5 nm and the length ranges between 8 and

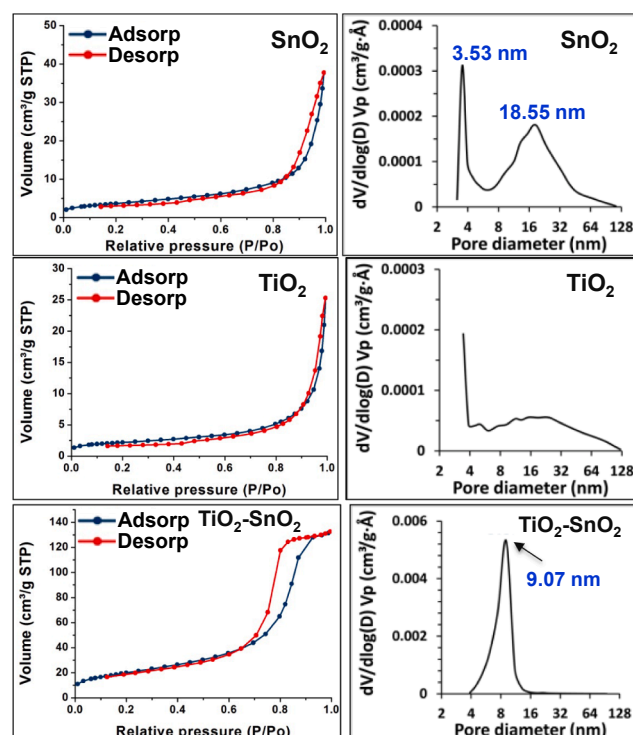


Fig. 3. N_2 isotherms and BJH pore size distribution plots of the catalysts.

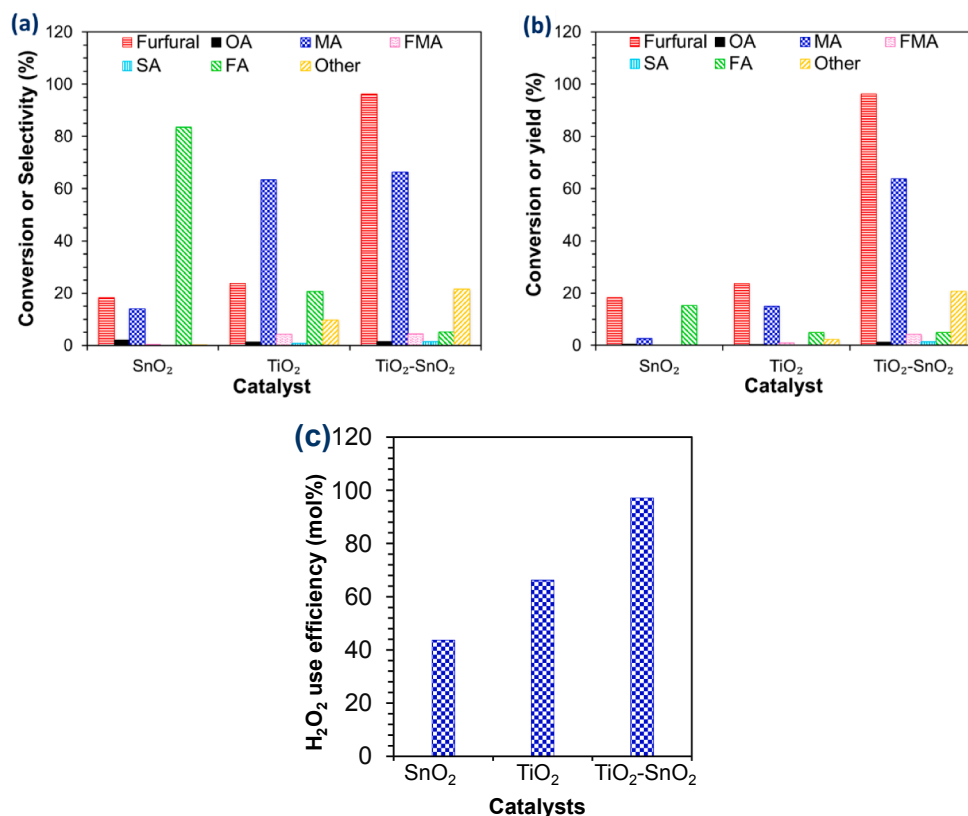


Fig. 4. Catalytic activity screening results of TiO₂-SnO₂ catalysts in the oxidation of furfural. (a) Selectivity; (b) Yield; and (c) H₂O₂ utilization efficiency. Reaction conditions: furfural (5 mmol), 30% (aq) H₂O₂ (25 mmol), catalyst (100 mg), T = 60 °C, t = 24 h, 10 ml co-solvent of H₂O (5 ml) and CH₃CN (5 ml) was used. Symbols: OA = oxalic acid; MA = maleic acid; SA = succinic acid; FA = furoic acid.

10 nm. The TiO₂-SnO₂ catalyst shows the morphology similar to that of SnO₂ NPs but with less agglomeration, which corroborate its high surface area and porosity compared to the single oxides (Table 1). The selected area electron diffraction (SAED) patterns are characterized by the diffraction rings, which indicate the polycrystalline nature of the heterostructure catalyst. The diffraction rings of SnO₂ and TiO₂-SnO₂ catalysts comprises discrete spots, whereas those of TiO₂ are more diffused which indicate amorphous phase. The three most inner indicated SAED rings for SnO₂ and TiO₂-SnO₂ catalysts correspond to the respective (1 1 0), (1 0 1) and (2 1 1) planes of the SnO₂ tetragonal phase, which are in agreement with the XRD (Fig. 1a) showing predominantly the SnO₂ reflection peaks. In addition to the three rings, there is a fourth ring corresponding to the SnO₂ (1 1 2) plane for SnO₂ and SnO₂ (3 0 1) plane for TiO₂-SnO₂. The diffraction ring for anatase (1 1 2) was observed for TiO₂-SnO₂. The indexed rings for TiO₂ correspond to the respective (2 0 0), (2 0 4) and (2 1 5) planes of anatase.

BET surface areas of 13.2 m²/g, 7.6 m²/g and 72.6 m²/g were measured for TiO₂, TiO₂ and TiO₂-SnO₂, respectively (Table 1). The pore diameter of TiO₂-SnO₂ is 11.0 nm while of TiO₂ and SnO₂ are respectively 9.0 nm and 9.5 nm. Further, TiO₂-SnO₂ shows higher pore volume of 0.20 cm³/g compared to 0.031 and 0.017 cm³/g for SnO₂ and TiO₂, respectively. The high surface area of TiO₂-SnO₂ correspond to the formation of nanosized particles comparable to single oxides as evidenced by the TEM images with size diameter of 10–20 nm (Fig. 2).

The adsorption–desorption isotherms and pore size distribution plots of the catalysts are presented in Fig. 3. The TiO₂-SnO₂ catalysts shows the type IV with classified H2 hysteresis loops characteristic of mesoporous materials [30]. This type of isotherm is an indication of the particles forming agglomerates arranged in a uniform way that have pores with narrow mouths and relatively uniform channel-like pores. The mesoporous character of the heterostructured the TiO₂-SnO₂ composite nanocatalyst was confirmed further by the pore size distribution,

which is narrow and uniformly distributed within the range 46 nm with the average centred at 9.07 nm. SnO₂ broad distributed pores sizes centred at both 3.53 nm and 18.55 nm while of TiO₂ are in the range of 420 nm.

Fig. 4 shows the comparison results of the catalytic performance of the TiO₂-SnO₂ catalysts in the furfural oxidation reaction. SnO₂ obtained the furfural conversion of 18.3% and maleic acid selectivity of 14.1% while TiO₂ afforded 23.7% furfural conversion and maleic acid selectivity of 63.4% (Fig. 4a). Further, SnO₂ showed high selectivity of 83.5% towards 2-furoic acid while TiO₂ did not (20.7%). Both SnO₂ and TiO₂ also showed the formation of fumaric acid, oxalic acid, and succinic acid at low selectivity. The TiO₂-SnO₂ catalyst exhibited a markedly improved catalytic activity with furfural conversion of 96.2% when compared to SnO₂ and TiO₂. The obtained high furoic acid selectivity of 83.5% for SnO₂ decreased significantly for TiO₂-SnO₂ to 5.1%. TiO₂-SnO₂ obtained a maleic acid formation yield of 63.8% at selectivity of 66.3% (Fig. 4a). Fig. 4c shows the H₂O₂ consumption amounts of the respective SnO₂, TiO₂ and TiO₂-SnO₂ catalysts in the oxidation reaction of furfural. The high-consumed amount of H₂O₂ was obtained with the TiO₂-SnO₂ catalyst, which also gave the highest conversion amount of furfural, thus yield of maleic acid. This high activity of TiO₂-SnO₂ is due to its enhanced redox activity manifested by the modified structure interactions of the two metal oxides. The participation of H₂O₂ in furfural oxidation reaction can be related to the typical Fenton-like driven catalytic radical's species, which form the active oxygen species such as hydroxyl following the involvement of Ti⁴⁺/Ti³⁺ redox cycle mechanism outlined below:



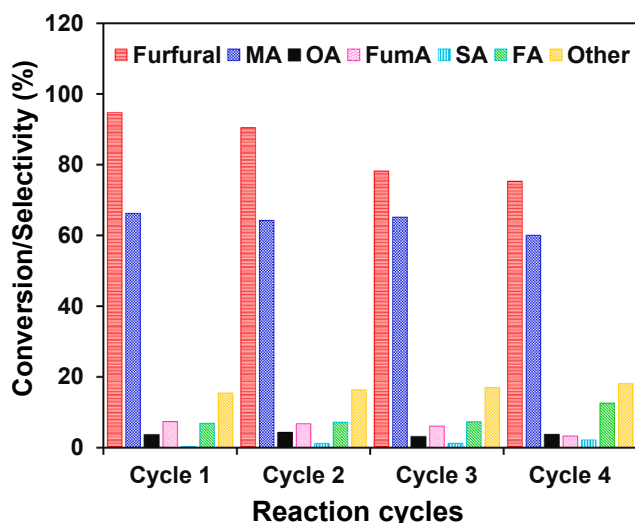


Fig. 5. Recyclability performance test of $\text{TiO}_2\text{-SnO}_2$ catalyst in furfural oxidation reaction. Reaction conditions: furfural (5 mmol), 30% (aq) H_2O_2 (25 mmol), catalyst (100 mg), $T = 60^\circ\text{C}$, $t = 24\text{ h}$, 10 ml co-solvent of H_2O (5 ml) and CH_3CN (5 ml) was used. Symbols: OA = oxalic acid; MA = maleic acid; SA = succinic acid; FA = furoic acid.

In first step, H_2O_2 is decomposed by $\text{Ti}^{4+}/\text{Ti}^{3+}$ of the $\text{TiO}_2\text{-SnO}_2$ catalyst to form highly reactive hydroxyl species during the reaction based on Eqs. (1) and (2). The formed hydroxyl species are reactive to activate the furfural molecule to undergo several functional groups rearrangements, which include the subsequent trapping of the oxygen species from the available hydroxyl source to stable oxygenated molecules as products. The XPS (Fig. S2) and EPR (Fig. 1e) showed the $\text{TiO}_2\text{-SnO}_2$ catalyst to possess high amount of surface oxygen defects than TiO_2 and SnO_2 , which was beneficial for the effective furfural conversions and at high preserved maleic acid selectivity and yields. The redox activity of surface exposed $\text{Ti}^{4+}/\text{Ti}^{3+}$ has also showed previously to be effective to facilitate the enhanced electrons transfer mobility in H_2O_2 mediated oxidation reactions [31]. Further, the high surface area of $\text{TiO}_2\text{-SnO}_2$ could also effect a significant textural property on catalytic performance (Table 1). According to XPS, the interfaced $\text{TiO}_2\text{-SnO}_2$ exist more in their higher oxidation states which presents a fully oxidised catalyst required to facilitate effective electron-transfer redox exchange for oxidation of furfural. The interfaced-enhanced catalytic performance of Ti and Sn oxide indicate the possible synergistic effect of the heterostructure catalyst for the efficient conversion of furfural to maleic acid with better selectivity, the similar synergistic effect has been previously reported elsewhere [32,33]. Hence, it present the opportunity for further studies to investigate a wide range effect of Ti:Sn compositions on the structure interface properties and their optimized structure-activity relationship performance in the furfural oxidation to maleic acid. This will include redox and acidic/basic active sites in conjunction with the surface oxygen vacancies. The recyclability performance of the $\text{TiO}_2\text{-SnO}_2$ catalyst in liquid phase oxidation of furfural under the co-solvent of acetonitrile/water. As illustrated in Fig. 5 the furfural conversion activity of the catalyst showed to drop gradually with each recycling while selectivity of towards maleic acid remain in a range of 6266%. The observed gradual decline in selectivity would require detailed study such as possible leaching caused by the acidic solvent effect, thus leading to catalytic activity reduction as has been demonstrated before due to the effect of the solvent [31].

4. Conclusion

In conclusion, we herein showed an effective catalytically active $\text{TiO}_2\text{-SnO}_2$ interfaced nano-oxide catalyst for the selective oxidation of

furfural to maleic acid. The structural interface of TiO_2 and SnO_2 displayed a synergistic catalytic activity enhancement due to the modified electronic structures, which is manifested by effective redox cycles and oxygen vacancies than the single oxide counterpart. The $\text{TiO}_2\text{-SnO}_2$ catalyst gave a furfural conversion of 96.2% to obtain maleic acid yield of 63.8% at 66.3% selectivity. Characterisation results showed that the enhanced catalytic performance was due to the structure effect from the oxygen vacancies, and improved redox reactive species. Both TiO_2 and SnO_2 are cheap and abundantly available metals, which can present an economical catalytic process for upgrade of biomass-derived furfural into renewable biobased maleic acid synthesis.

CRedit authorship contribution statement

Petrus M. Malibo: Formal analysis, Methodology, Investigation, Visualization, Writing - original draft. **Peter R. Makgwane:** Conceptualization, Investigation, Validation, Resources, Funding acquisition, Supervision, Project administration, Writing - review & editing. **Priscilla G.L. Baker:** Conceptualization, Writing - review & editing, Supervision.

Declaration of Competing Interest

The authors declare that they have no known competing financial interests or personal relationships that could have appeared to influence the work reported in this paper.

Acknowledgements

CSIR-SRP thematic (grant number T#18/2019-2020) is thanked for the financial support. The financial support for analysis of XPS samples from Dr M.M. Mphahlele-Makgwane (University of Limpopo) is acknowledged.

Appendix A. Supplementary material

Supplementary data to this article can be found online at <https://doi.org/10.1016/j.inoche.2021.108637>.

References

- [1] R. Wojcieszak, F. Santarelli, S. Paul, F. Dumeignil, F. Cavani, R.V. Gonçalves, Recent developments in maleic acid synthesis from bio-based chemicals, *Sustain. Chem. Process.* 3 (2015) 9–20, <https://doi.org/10.1186/s40508-015-0034-5>.
- [2] M.L. Granados, J. Moreno, A.C. Alba-Rubio, J. Iglesias, D.M. Alonso, R. Mariscal, Catalytic transfer hydrogenation of maleic acid with stoichiometric amounts of formic acid in aqueous phase: paving the way for more sustainable succinic acid production, *Green. Chem.* 22 (2020) 1859–1872, <https://doi.org/10.1039/C9GC04221K>.
- [3] M.Y. Byun, J.S. Kim, J.H. Baek, D.W. Park, M.S. Lee, Liquid-phase hydrogenation of maleic acid over Pd/ Al_2O_3 catalysts prepared via deposition-precipitation method, *Energies* 12 (2019) 284, <https://doi.org/10.3390/en12020284>.
- [4] T.R. Felthouse, J.C. Burnett, B. Horrell, M.J. Mummey, Y.J. Kuo, Maleic anhydride, maleic acid, and fumaric acid, in: J. Kroschwitz, M. Home-Grant (Eds.), *Kirk-Othmer Encyclopedia of Chemical Technology*, John Wiley and Sons, New York, 2001, pp. 1–58.
- [5] D.K. Hood, O.M. Musa, *Progress in maleic anhydride production*, in: O.M. Musa (Ed.), *Handbook of maleic anhydride based materials: Syntheses, properties and applications*, Springer International Publishing, Cham, Switzerland, 2016, pp. 3–35.
- [6] P. Santander, L. Bravo, G. Pecchi, A. Karelavic, The consequences of support identity on the oxidative conversion of furfural to maleic anhydride on vanadia catalysts, *Appl. Catal. A: Gen.* 5955 (2020), 117513, <https://doi.org/10.1016/j.apcata.2020.117513>.
- [7] S. Shi, H. Guo, G. Yin, Synthesis of maleic acid from renewable resources: catalytic oxidation of furfural in liquid media with dioxygen, *Catal. Comm.* 12 (2011) 731–733, <https://doi.org/10.1016/j.catcom.2010.12.033>.
- [8] M. Rezaei, A.N. Chermahini, H.A. Dabagh, M. Saraji, A. Shahvar, Furfural oxidation to maleic acid with H_2O_2 by using vanadyl pyrophosphate and zirconium pyrophosphate supported on well-ordered mesoporous KIT-6, *J. Environ. Chem. Eng.* 7 (2019), 102855, <https://doi.org/10.1016/j.jece.2018.102855>.
- [9] Y. Xie, Y. Huang, C. Wu, W. Yuan, Y. Xia, X. Liu, H. Wang, Iron-based metalloporphyrins as efficient catalysts for aerobic oxidation of biomass derived furfural

- into maleic acid, *Mol. Catal.* 452 (2018) 20–27, <https://doi.org/10.1016/j.mcat.2018.03.018>.
- [10] N. Alonso-Fagúndez, V. Laserna, A.C. Alba-Rubio, M. Mengibar, A. Heras, R. Mariscal, M.L. Granados, Granados. Poly-(styrene sulphononic acid): An acid catalyst from polystyrene waste for reactions of interest in biomass valorization, *Catal. Today* 234 (2014) 285–294, <https://doi.org/10.1016/j.cattod.2014.01.041>.
- [11] N. Alonso-Fagúndez, I. Agirrezabal-Telleria, P.L. Arias, J.L.G. Fierro, R. Mariscal, M.L. Granados, Aqueous-phase catalytic oxidation of furfural with H₂O₂: high yield of maleic acid by using titanium silicalite-1, *RSC Adv.* 4 (2014) 54960–54972, <https://doi.org/10.1039/C4RA11563E>.
- [12] T. Soták, M. Hronec, M. Gál, E. Dobročka, J. Škriniarová, Aqueous-phase oxidation of furfural to maleic acid catalyzed by copper phosphate catalysts, *Catal. Lett.* 147 (2017) 2714–2723, <https://doi.org/10.1007/s10562-017-2191-5>.
- [13] M.J. da Silva, A.A. Rodrigues, Silicotungstate salts as catalysts in furfural oxidation reactions with hydrogen peroxide, *Mol. Catal.* (2020), 111104, <https://doi.org/10.1016/j.mcat.2020.111104>.
- [14] S.K. Pillai, O. Gheevarghese, S. Sugunan, Catalytic properties of V₂O₅/SnO₂ towards vapour-phase Beckmann rearrangement of cyclohexanone oxime, *Appl. Catal. A: Gen.* 353 (2009) 130–136, <https://doi.org/10.1016/j.apcata.2008.10.033>.
- [15] P.R. Makgwane, S.S. Ray, Development of a high-performance nanostructured V₂O₅/SnO₂ catalyst for efficient benzene hydroxylation, *Appl. Catal. A: Gen.* 492 (2015) 10–22, <https://doi.org/10.1016/j.apcata.2014.12.024>.
- [16] S. Zhong, Y. Xi, Q. Chen, J. Chen, S. Bai, Bridge engineering in photocatalysis and photoelectrocatalysis, *Nanoscale* 12 (2020) 5764–5791, <https://doi.org/10.1039/C9NR10511E>.
- [17] S. Zhong, Y. Xi, S. Wu, Q. Liu, L. Zhao, S. Bai, Hybrid cocatalysts in semiconductor-based photocatalysis and photoelectrocatalysis, *J. Mater. Chem. A* 8 (2020) 14863–14894, <https://doi.org/10.1039/D0TA04977H>.
- [18] S.S. Nkosi, I. Kortidis, D.E. Motaung, P.R. Makgwane, O.M. Ndwandwe, S.S. Ray, G. Kiriakidis, An instant photo-excited electrons relaxation on the photo-degradation properties of TiO_{2-x} films, *J. Photochem. Photobiol. A: Chem.* 293 (2014) 72–80, <https://doi.org/10.1016/j.jphotochem.2014.07.012>.
- [19] E. Kolobova, Y. Kotolevich, E. Pakrieva, G. Mamontov, M.H. Farias, V. C. Corberánd, N. Bogdanchikova, J. Hemming, A. Smeds, P. Mäki-Arvela, D. Yu. Murzin, A. Pestryakov, Modified Ag/TiO₂ systems: Promising catalysts for liquid-phase oxidation of alcohols, *Fuel* 234 (2018) 110–119, <https://doi.org/10.1016/j.fuel.2018.06.128>.
- [20] Z. Wang, J. Feng, X. Li, R. Oh, D. Shi, O. Akdim, M. Xia, L. Zhao, X. Huang, G. Zhang, Au-Pd nanoparticles immobilized on TiO₂ nanosheet as an active and durable catalyst for solvent-free selective oxidation of benzyl alcohol, *J. Colloid Interf. Sci.* 588 (2021) 787–794, <https://doi.org/10.1016/j.jcis.2020.11.112>.
- [21] L. Li, C. Zhang, W. Chen, Fabrication of SnO₂-SnO nanocomposites with p-n heterojunctions for the low-temperature sensing of NO₂ gas, *Nanoscale* 7 (2015) 12133–12142, <https://doi.org/10.1039/C5NR02334C>.
- [22] F. Morazzoni, C. Canevali, N. Chiodini, C. Mari, R. Ruffo, R. Scotti, L. Armelao, E. Tondello, L.E. Depero, E. Bontempi, Nanostructured Pt-doped tin oxide films: Sol-gel preparation, spectroscopic and electrical characterization, *Chem. Mater.* 13 (2001) 4355–4361, <https://doi.org/10.1021/cm001228o>.
- [23] N. Kruse, S. Chenakin, XPS characterization of Au/TiO₂ catalysts: binding energy assessment and irradiation effects, *Appl. Catal. A: Gen.* 391 (2011) 367–376, <https://doi.org/10.1016/j.apcata.2010.05.039>.
- [24] Z. Li, W. Shen, X. Zhang, L. Fang, X. Zu, Controllable growth of SnO₂ nanoparticles by citric acid assisted hydrothermal process, *Colloids Surf. A Physicochem. Eng. Asp.* 327 (2008) 17–20, <https://doi.org/10.1016/j.colsurfa.2008.05.043>.
- [25] P.S. Bagus, E. Siltón, C.J. Nelin, The interpretation of XPS spectra: Insights into materials properties, *Surf. Sci. Rep.* 68 (2013) 273–304.
- [26] G. Greczynski, L. Hultman, X-ray photoelectron spectroscopy: Towards reliable binding energy referencing, *Prog. Mater. Sci.* 107 (2020), 100591.
- [27] T.C. Taucher, I. Hehn, O.T. Hofmann, M. Zharnikov, E. Zojer, Understanding chemical versus electrostatic shifts in X-ray photoelectron spectra of organic self-assembled monolayers, *J. Phys. Chem. C* 120 (2016) 3428–3437.
- [28] N.M. Dimitrijevic, Z.V. Saponjic, B.M. Rabatic, O.G. Poluektov, T. Rajh, Effect of size and shape of nanocrystalline TiO₂ on photogenerated charges, An EPR study, *J. Phys. Chem. C* 111 (2007) 14597–14601, <https://doi.org/10.1021/jp0756395>.
- [29] D.C. Hurum, A.G. Agrios, K.A. Gray, T. Rajh, M.C. Thurnauer, Explaining the enhanced photocatalytic activity of Degussa P25 mixed-phase TiO₂ using EPR, *J. Phys. Chem. B* 107 (2003) 4545–4549, <https://doi.org/10.1021/jp0273934>.
- [30] L. Zhu, Z. Yang, J. Zheng, W. Hu, N. Zhang, Y. Li, C.J. Zhong, H. Ye, B.H. Chen, Decoration of Co/Co₃O₄ nanoparticles with Ru nanoclusters: A new strategy for design of highly active hydrogenation, *J. Mater. Chem. A* 3 (2015) 11716–11719, <https://doi.org/10.1039/C5TA02452H>.
- [31] A.C. Alba-Rubio, J.L.G. Fierro, L. León-Reina, R. Mariscal, J.A. Dumesic, M. L. Granados, Oxidation of furfural in aqueous H₂O₂ catalysed by titanium silicalite: Deactivation processes and role of extraframework Ti oxides, *Appl. Catal. B: Environ.* 202 (2017) 269–280, <https://doi.org/10.1016/j.apcatb.2016.09.025>.
- [32] L. Zhu, Y. Jiang, J. Zheng, N. Zhang, C. Yu, Y. Li, C.W. Pao, J.L. Chen, C. Jin, J. F. Lee, C.J. Zhong, Ultrafine nanoparticle-supported Ru nanoclusters with ultrahigh catalytic activity, *Small* 11 (2015) 4385–4393, <https://doi.org/10.1002/sml.201500654>.
- [33] L. Zhu, H. Zhang, N. Ma, C. Yu, N. Ding, J.L. Chen, C.W. Pao, J.F. Lee, Q. Xiao, B. H. Chen, Tuning the interfaces in the ruthenium-nickel/carbon nanocatalysts for enhancing catalytic hydrogenation performance, *J. Catal.* 377 (2019) 299–308, <https://doi.org/10.1016/j.jcat.2019.07.041>.